This is an open access article published under an ACS AuthorChoice License, which permits copying and redistribution of the article or any adaptations for non-commercial purposes.

ACS OMEGA

Article

Cite This: ACS Omega 2019, 4, 6218−6228

http://pubs.acs.org/journal/acsodf

Selective Detection of Trinitrophenol by Amphiphilic Dimethylaminopyridine-Appended Zn(II)phthalocyanines at the Near-Infrared Region

S. Kasthuri,[†] Pratiksha Gawas,[†] Samarendra Maji,[†] N. Veeraiah,[‡] and N. Venkatramaiah*[,†]

[†]Department of Chemistry, SRM Institute of Science and Technology (SRMIST), Chennai 603 203, India

[‡]Department of Physics, Acharya Nagarjuna University, Nagarjuna Nagar, Guntur 522 510, Andhra Pradesh, India

Supporting Information

ABSTRACT: Novel amphiphilic Zn(II)phthalocyanines (ZnPcs) peripherally substituted with four and eight dimethylaminopyridinium units (ZnPc**1** and ZnPc**2**) were synthesized by cyclotetramerization of the corresponding phthalonitriles. The effect of aggregation and photophysical (fluorescence quantum yields and lifetimes) and photochemical (singlet oxygen generation and photodegradation under light irradiation) properties was investigated. The chemosensing ability of ZnPcs toward explosive nitroaromatic compounds was explored in aqueous medium. This study demonstrates that ZnPc**1** and ZnPc**2** show fluorescence quenching behavior upon interaction with different nitro analytes and show unprecedented selectivity toward 2,4,6-trinitrophenol with a limit of detection (LOD) of 0.7−1.1 ppm with a high quenching rate constant (K_{sv}) of 1.6−2.02 × 10^5. The near-infrared (NIR) fluorescence in thin films was quenched efficiently because of the photoinduced electron-transfer process through strong intermolecular $\pi-\pi$ and electrostatic interactions. The sensing process is highly reversible and free from the interference of other commonly encountered nitro analytes. Further, experiments were performed to demonstrate the use of ZnPcs as efficient heterogeneous photocatalysts in the reduction of nitro explosives. The smart dual performance of multicharged ZnPcs in aqueous media quantifies them as attractive candidates in developing sensor materials at the NIR region and to possibly convert the toxic explosives into useful scaffolds. These results provide an interesting perspective toward elaboration of stable fluorescent systems for the selective sensing behavior of nitro explosives and their facile heterogeneous catalytic behavior in the reduction reactions.

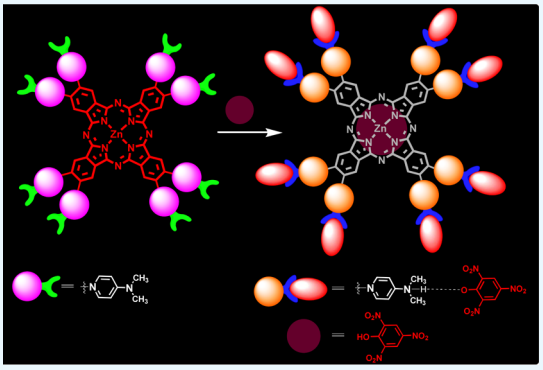

INTRODUCTION

In recent years, significant research efforts have been made to develop chemical sensors for explosive compounds toward security and environment protection. Long-term disposal of explosives such as nitroaromatic compounds, related nitrated explosives, and their degraded products has shown detrimental effects on the human health and also enhanced the toxic levels of soil and groundwater.[1,2] For example, 2,4,6-trinitrophenol (TNP) [also known as picric acid (PA)] was extensively used in the manufacture of rocket fuel, fireworks, textile industry, and astringent for the medical purpose. TNP and its biologically transformed products such as picramic acids have been identified as highly toxic species to biota and lead to chronic diseases such as sycosis and cancer.[3] Different analytical techniques have been employed for the detection of explosives, such as ion mobility spectroscopy, neutron activation analysis, chromatography, infrared spectroscopy, electrochemical detection, surface-enhanced Raman spectroscopy, and X-ray imaging.[4−9] Most of these methods pose difficulties in the trace detection of explosives, complicated manipulation, preconcentration prior to the analysis, and operation difficulty. Currently available detection devices cannot be assembled in a small and low-power package for field analysis, thus restricting the popularization toward the recognition of explosives. Recently, optical methods based on colorimetric and fluorescence changes have gained much attention because of their high selectivity and fast detection in both solid and liquid phases and can be easily incorporated into inexpensive and portable microelectronic devices. Suslick and Lin have developed an array-based colorimetric sensor system for triacetone triperoxide and other explosive analytes with different redox indicators by a color recognition pattern with a limit of detection (LOD) below 2 ppb.[10] Different fluorescent probes such as conjugated polymers, small fluorescent molecules, quantum dots, metal−organic frameworks (MOFs), and covalent organic frameworks were used for the detection of explosives.[11−14] The predominant detection mechanism and high sensitivity are endorsed because

Received: September 15, 2018
Accepted: March 25, 2019
Published: April 3, 2019

© 2019 American Chemical Society

DOI: 10.1021/acsomega.8b02394
ACS Omega 2019, 4, 6218−6228

Scheme 1. Synthetic Route for the Preparation of DMAP-Appended ZnPcs

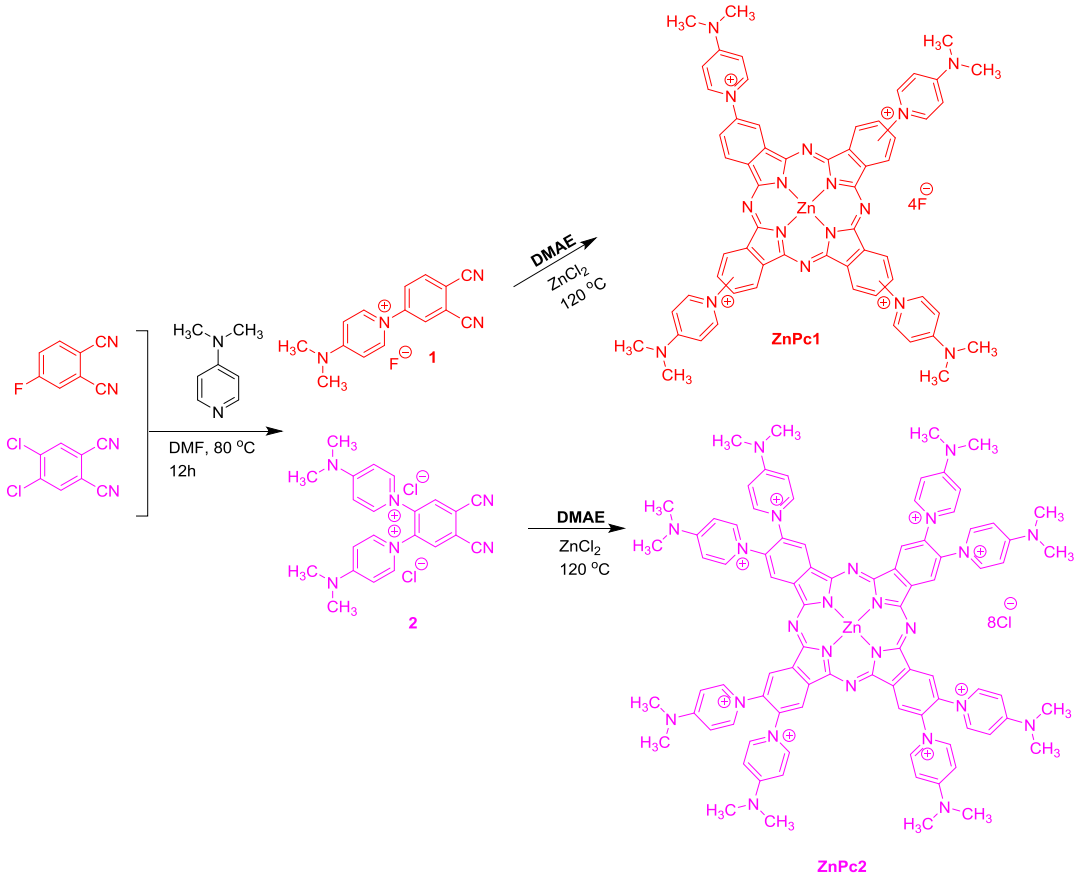

of strong $\pi-\pi$ interactions, inter/intra molecular hydrogen bonding, Meisenheimer complex, and electrostatic interactions between fluorophores and explosive analytes.[15−18] Xu et al. have developed an infrared emission probe DNSA-SQ, which shows turn-on fluorescence upon interaction with PA by intramolecular charge transfer along with protonation of the dimethylamine group by PA.[19] Ghosh et al. have developed a porous UiO-68@NH_2 MOF containing pendant Lewis basic amine recognition sites. The obtained MOF show high selective recognition for TNP in a few seconds with 23 times high quenching rate than 2,4,6-trinitrotoluene (TNT) and $(O_2NNCH_2)_3$. The phenolic −OH of TNP undergoes electrostatic interactions with the $-NH_2$ unit of MOFs along with the energy-transfer mechanism.[20] Bhalla et al. have developed nanoaggregates of supramolecular assembly of a hexaphenylbenzene derivative modulated with Hg^{2+} ions, which show remarkable selectivity for TNP because of transfer of protons of hydroxyl groups to the basic *N*,*N*-dimethylamino group to make an electrostatic complex between host and guest.[21] Literature studies in the field of explosive sensors have allowed the realization of highly sensitive sensors; however, novel functionalization of amphiphilic molecular ensembles for selective detection of explosive analytes in aqueous medium at the near-infrared (NIR) region with high sensitivity is very limited. Phthalocyanines (Pcs) are a class of high π-conjugated systems with an intense absorption at the visible and NIR region with high photostability/thermal stability, which makes them active photosensitizers in photodynamic therapy.[22,23] Because of low solubility of Pcs in common solvents, their physico-chemical properties are prevented from being extensively used in technological applications. However, their solubility can be improved by attaching some functional groups such as −COOH, $-SO_3H$, $-PO_3H_2$, ammonium, long alkyl, alkoxy, phenoxy groups, and crown ethers at peripheral and nonperipheral positions and/or by inserting some metal atoms in the inner core of the ring.[24−27] Modified metallo phthalocyanines (MPcs) were exploited toward optical sensors for volatile organic compounds. MPcs modified with fluoroalkyl substituents and the metal ion showed an increased sensitivity and selectivity toward TNT by the quartz crystal microbalance method.[28] The high planar nature of Pcs promotes strong interactions with acceptor molecules by formation of strong $\pi-\pi$ stacking interactions, leading to dramatic changes in the Q-band absorption and emission properties. Introduction of a varied number of amine functionalities on Zn(II)phthalocyanines (ZnPcs) shows selective sensing behavior of TNP, which arises because of increase in the donating strength on ZnPcs for efficient $\pi-\pi$ stacking with TNP in chloroform and vapor-phase methods.[29] However, the aqueous phase detection of TNP becomes an imperative aspect for the design of potential sensors because of its high water solubility (∼14 g/L at 20 °C) and low octanol−water partition coefficient (log K_{ow} = 1.6).[30] To the best of our knowledge, the design of explosive chemical sensors in aqueous medium at the NIR region is very limited. The fluorescent sensors at the NIR region has significant advantages over the visible region because of lower photo damage and reduced light scattering and can effectively avoid background interference to enhance the selectivity and sensitivity. In this work, we describe a facile synthesis of

DOI: 10.1021/acsomega.8b02394
ACS Omega 2019, 4, 6218−6228

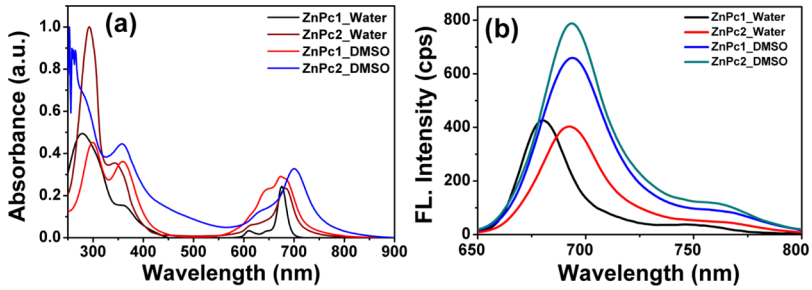

Figure 1. (a) Absorption spectra of ZnPcs in different solvents. (b) Emission spectra of ZnPcs upon excitation at λ_{ex} = 630 nm.

novel amphiphilic Zn(II)Pcs with varied number of dimethylaminopyridinium (DMAP) units at peripheral positions. Nucleophilic substitution of DMAP units on Zn(II)Pcs imparts positive charge on the macromolecule to enhance the solubility in aqueous medium and extended conjugation by strongly influencing the photophysical properties at the near NIR region. The compounds show high photostability and could be able to generate high singlet oxygen ($^1O_2$). The chemosensing ability of ZnPcs with different explosive nitroaromatic compounds (NACs) is demonstrated in aqueous and vapor-phase methods. ZnPc**2** shows unprecedented selectivity toward TNP and shows turn-off fluorescence by efficient $\pi-\pi$ interactions and intramolecular charge processes by protonating the dimethylamine group. Moreover, the utility of ZnPc**2** as a photocatalyst in the reduction of TNP is demonstrated with an emphasis of dual behavior of the molecular ensemble for the selective sensing behavior of nitro explosives which are converted into useful building blocks to develop macromolecules.

RESULTS AND DISCUSSION

The detailed synthetic methodology adopted for the preparation of water-soluble ZnPc derivatives with four and eight units of 4-dimethylaminopyridine (DMAP) (ZnPc**1**−**2**) is described in Scheme 1. Precursor mono- and disubstituted dimethylaminopyridinium phthalonitriles (1 and 2) were obtained by the nucleophilic substitution of DMAP with corresponding halogenated phthalonitriles in anhydrous dimethylformamide (DMF) at 80 °C under N_2 atmosphere for 12 h. The formation of the precipitate was observed during the reaction, which indicates the nucleophilic substitution of the DMAP unit on phthalonitriles.[32] The cyclotetramerization of 4-dimethylaminopyridinium phthalonitriles was carried out in 2-dimethylaminoethanol at 120 °C in the presence of anhydrous $ZnCl_2$ and catalytic amount of DBU under N_2 atmosphere. The reaction mixture was precipitated by adding acetone and methanol solvent mixtures. The peripheral 4-(dimethylamino)pyridine-substituted ZnPcs**1**−**2** were obtained in good yields (58−63%), which exhibit good solubility in water. A detailed synthetic procedure is described in the Supporting Information. ZnPc**1** was obtained in a mixture of four possible structural isomers. The four probable isomers can be designated by their molecular symmetry as C_{4h}, C_{2v}, C_s, and D_{2h}.[33] The structure of the final target compounds was confirmed by nuclear magnetic resonance (NMR), Fourier transform infrared (FT-IR), and mass analysis. The ^{1}H NMR spectrum of phthalonitrile, **1**, shows a singlet peak of $-N(CH_3)_2$ at δ 3.21 ppm and two doublet peaks of DMAP at δ 8.03 (Py-*o*-H) and 8.01 (Py-*m*-H). Phthalonitrile, **2**, shows two doublet peaks at δ 8.38 (Py-*o*-H) and 7.21 (Py-*m*-H) corresponding to the aromatic region of DMAP and a singlet peak at δ 3.27 corresponds to $-N(CH_3)_2$. The electrospray ionization mass spectrometry (MS) spectra show the molecular ion peaks at 249.1 and 370.2 [M^+], corroborating the proposed structure of phthalonitriles. The ^{1}H NMR spectrum of ZnPc**1** in DMSO-d_6 shows four different multiplets corresponding to four different isomers. The pyridyl protons of Py-*o*-H, Py-*m*-H, and Pc-H (α and β) appear as broad multiplets at δ 8.24−8.18, 7.95−7.86, 7.58−7.44, and 6.97−6.92 ppm and of $-N(CH_3)_3$ groups appear as a singlet peak at δ 3.17 ppm. Because of the symmetrical nature of ZnPc**2**, the aromatic protons of pyridinium groups appear as doublets at δ 8.27 (Py-*o*-H) and 7.03 ppm (Py-*m*-H). The proton signals of Pc-α-H appear as broad peaks at δ 8.75 and 7.36 ppm and of $-N(CH_3)_3$ groups appear at δ 3.23 ppm. The high-resolution MS spectra of ZnPc**1** and ZnPc**2** show molecular ion peaks at 268.10730 and 265.10732, respectively, corresponding to $[M + 1]^{4+}$ and $[M - (DMAP)_4]^{4+}$, corroborating in tandem the structural features of the desired compounds (Figures S1−S10, Supporting Information).

The FT-IR spectra of phthalonitriles show a $-C\equiv N$ stretching band at ca. 2248−2236 cm^{-1}, which disappeared in the macrocycle, indicating the complete conversion of phthalonitriles into ZnPcs. For ZnPc**1** and ZnPc**2**, the characteristic macrocycle torsional and wagging vibrations of C−H groups appear at ca. 2924−2930 cm^{-1}, and C=C modes appear at 1649 cm^{-1}. The absorption of variant C=N in the phthalocyanine ring observed at 1572 cm^{-1} and C−C isoindole ring stretching vibrations are in the range of ca. 1394−1341 cm^{-1} (Figure S11, Supporting Information). The UV−visible absorption spectra of Zn(II)Pcs exhibited characteristic absorptions in the Q-band region at 680−710 nm, which are attributed due to $\pi \rightarrow \pi^*$ transitions from the highest occupied molecular orbital (HOMO) to the lowest unoccupied molecular orbital (LUMO) of the complexes. The B-band appeared at 300−360 nm, which arises from the deeper $\pi \rightarrow \pi^*$ transition of HOMO (a_{1u} and a_{2u}) to LUMO (e_g). Both ZnPc**1** and ZnPc**2** are well soluble in water, dimethyl sulfoxide (DMSO), and DMF and partially soluble in ethanol. Figure 1a shows the absorption spectra of ZnPcs**1**−**2** in water and DMSO solutions. ZnPc**1** shows an intense absorption band at 678 nm along with another band at 609 nm. ZnPc**2** shows Q-band absorption at 683 nm along with a broad shoulder peak at 616 nm, indicating that compounds are exhibited in monomeric form in water.[34] In DMSO, the Q-bands were broadened and slightly red-shifted. ZnPc**2** exhibits an ∼20 nm red shift in comparison to ZnPc**1**. On the other hand, ZnPcs**1**−**2** show B-band absorption at ca. 345−362 nm with variations in the absorption coefficient. The absorption

DOI: 10.1021/acsomega.8b02394
ACS Omega 2019, 4, 6218−6228

Table 1. Summary on Photophysical Properties of ZnPcs in DMSO

	absorption (nm)						
compound	B-band	Q-band	emission λ_{ex} = 630 nm	fluorescence Q.Y[a]	lifetime, ns	K_r (ns^{-1})[b]	K_{nr} (ns^{-1})[c]
ZnPc**1**	299, 360	644, 681	684, 752	0.11	2.89	0.038	0.307
ZnPc**2**	281, 359	632, 701	696, 761	0.16	2.78	0.057	0.302

[a]Reference to ZnPc (Φ_f) = 0.20. [b]$K_r = \Phi_f/\tau_F$. [c]$K_{nr} = 1 - \Phi_f/\tau_F$.

peak at 281−291 nm is in correlation to the absorption of DAMP because of transitions from the deeper π-levels.

Fluorescence emission spectra of ZnPcs were recorded in DMSO and water upon excitation at λ_{ex} = 630 nm (Figure 1b). The emission spectrum of ZnPc**1** shows emission maxima at 684 nm, and ZnPc**2** shows a red-shifted emission at ca. 15 nm in comparison to ZnPc**1**, which reveals that increase in the number of DMAP units on ZnPc increases its conjugation and furnishes a bathochromic shift in the absorption and emission spectra. In DMSO, the emission intensity is broadened and shows emission maxima at 693 and 696 nm for ZnPc**1** and ZnPc**2**, respectively. The fluorescence lifetime of ZnPc**1** and ZnPc**2** exhibits 2.890 ± 0.03 and 2.78 ± 0.02 ns, respectively, using the time-correlated single-photon counting (TCSPC) method (Figure S12, Supporting Information). Quantum yields (Φ_f) of the ZnPc derivatives were measured in the DMSO solution with reference to ZnPc. The quantum yields were found to be 0.11 and 0.16 for ZnPc**1** and ZnPc**2**, respectively. Table 1 summarizes the photophysical data of ZnPcs in DMSO.

The aggregation behavior of ZnPcs was studied in phosphate-buffered saline (PBS) and DMSO as a function of the concentration, and changes in B- and Q-band absorbance were monitored. Figure S13a (Supporting Information) shows the absorption spectra of ZnPcs in DMSO at different concentrations (2−20 μM). A linear increase was observed in the intensity of B-band and Q-band at 299, 360, and 681 nm for ZnPc**1**. Interestingly, ZnPc**2** shows a new broad peak at 759 nm. The intensity of peak gradually increased with an increase in the concentration of ZnPc**2**, revealing the formation of J-aggregates. The intensity of both B- and Q-bands at 281, 359, and 701 nm increased linearly. The inset shows the change in the Q-band intensity for different concentrations. For both compounds, the Q-band absorbance increases linearly by following Beer−Lambert's law with the rate constants of 3.7 × 10^4 and 3.8 × 10^4. Under similar concentration ranges, these compounds showed a decrease in the Q-band intensities in the PBS solution, and the intensity of both B- and Q-bands followed a linear relation with the concentration (Figure S13b, Supporting Information).

The singlet oxygen generation ($^1O_2$) was studied by the chemical method using 1,3-diphenylisobenzofuran (DPBF) as a singlet oxygen scavenger. Change in the absorbance of DPBF was monitored upon irradiation of light in both the presence and absence of ZnPcs. During photolysis, we have not observed any significant changes in the Q-band intensities, confirming that ZnPcs do not undergo photodegradation during singlet oxygen formation and are quite stable under light irradiation.

The assays of stability and photostability of ZnPc**1** and ZnPc**2** upon irradiation with white and red lights (150 mW cm^{-2}) were carried out, and the results are summarized in Table S1 (Supporting Information). Both the compounds were able to produce $^1O_2$, and the photosensitizing ability was found to be higher for ZnPc**1** than for ZnPc**2**. ZnPc**1** shows 89% decrease in the DPBF absorbance over a total irradiation period of 25 min (Figure 2). The variation in $^1O_2$ is due to the

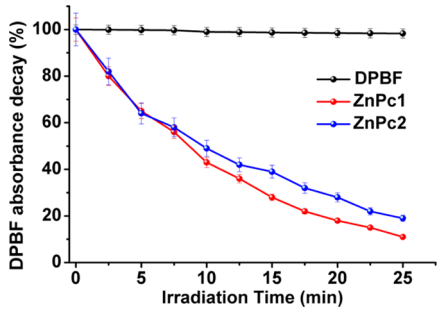

Figure 2. Time-dependent decomposition of DPBF (50 μM) photosensitized by ZnPcs in DMF/H_2O (9:1) upon irradiation with white light, filtered through a cutoff filter for λ < 540 nm at an irradiance of 9.0 mW cm^{-2} with (tests) or without (control) ZnPcs (0.5 μM). Values correspond to the average of three independent experiments.

formation of aggregates in ZnPc**2**. Since, the aggregation lowers the photo activity of molecules through dissipation of energy by aggregates in the excited state furnishes decrease in the formation of $^1O_2$.[34]

The electrochemical properties of ZnPcs were investigated by cyclic voltammetry with Ag/AgCl (3 M KCl) as the reference electrode (Figure 3). ZnPcs show reduction onset

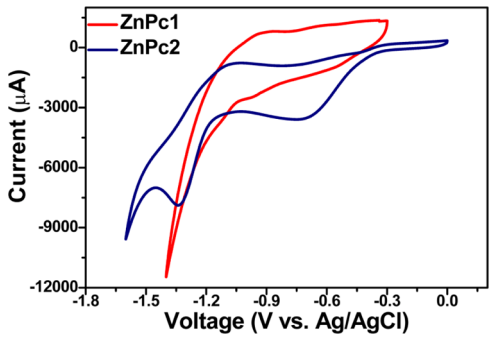

Figure 3. Cyclic voltammogram of ZnPcs (0.250 mM) in water.

potential with quasi-reversibility of two one electron-transfer processes: one in the region of ca. −0.57 to −0.97 V and the other in the region of ca. −1.18 to −1.08 V. The onset reduction $E_{1/2}$ values with respect to NHE are found to be −0.94 and −1.16 V for ZnPc**1** and −0.64 and −1.11 V for ZnPc**2**, respectively. The reduction potential of ZnPc**2** is less negative than that of ZnPc**1**, indicating that LUMO levels are significantly decreased by the increase in the number of DMAP units on ZnPcs, which facilitates more favorable electron-transfer process with acceptor molecules.

To obtain a deeper insight into understanding the electronic structures and the energy levels of ZnPcs, density function

DOI: 10.1021/acsomega.8b02394
ACS Omega 2019, 4, 6218−6228

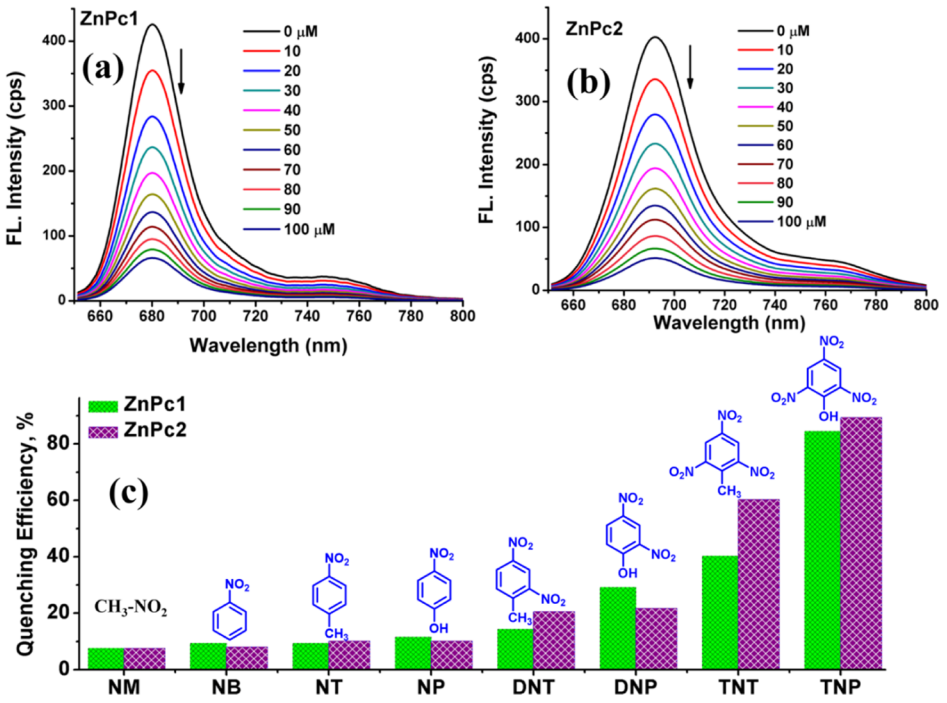

Figure 4. Change in the emission intensities of ZnPcs upon addition of different concentrations of TNP (a,b). (c) Change in the quenching efficiency of ZnPcs upon addition of different nitro analytes.

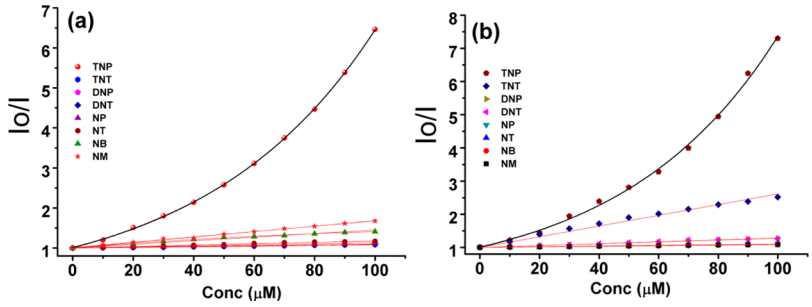

Figure 5. SV plot of ZnPc**1** (a) and ZnPc**2** (b) treated with different nitro analytes.

theory (DFT) calculations were carried out at the B3LYP/6-31g* basis set using Gaussian 16 package.[35] From the optimized geometry, the HOMO electron density is mainly localized on the macrocycle backbone and the LUMO electron density is distributed on the DMAP units present at the periphery. The calculated HOMO and LUMO energy levels are found to be −1.76 and −1.17 eV for ZnPc**1** and −0.91 and −0.49 eV for ZnPc**2**, respectively. The obtained energy levels from DFT studies are consistent with the electrochemical data. For ZnPc**2**, the LUMO energy levels decreased dramatically, leading to a decrease in the HOMO−LUMO gap (0.48 eV) and favoring easy transfer of electrons from ZnPcs to the acceptor molecule (Figure S14, Supporting Information).

The rich π-electronic nature and emission of ZnPcs in the red region, energy levels, and good solubility in aqueous medium provoke us to explore their potential application as fluorescent chemosensors at the NIR region. To study the interaction between nitro explosives and ZnPcs, fluorescence titration experiments were performed by adding aliquots of various analytes to the aqueous solution of ZnPcs. NACs are high electron-deficient compounds, which can undergo efficient $\pi-\pi$ and H-bonding interactions, furnishing a differential change in the emission properties. Different NACs such as nitrobenzene (NB), 4-nitrotoluene (NT), 4-nitrophenol (NP), 2,4-dinitrotoluene (DNT), 2,4-dinitrophenol (DNP), TNT, TNP, and nitromethane (NM) were treated with ZnPcs. Because of electron-deficient nature of the NACs, the fluorescence intensity of ZnPcs was readily quenched because of facile electron transfer between the fluorophore and NACs. However, the degree of quenching significantly varied with the nature of nitro analytes. The fluorescence titration experiments were carried out upon incremental addition of various nitroaromatics (with a concentration of $\sim 1 \times 10^{-6}$ to $\sim 2 \times 10^{-4}$ M) to the solution of ZnPcs ($\sim 2 \times 10^{-5}$ M). Figure 4a,b shows the change in the emission intensity of ZnPc**1** and ZnPc**2** (in H_2O) upon addition of TNP. For both compounds, we have observed ∼10% decrease in the emission intensity upon addition of 10 μM solution of TNP. The emission intensity changed dramatically upon initial addition and then reached a plateau. Upon addition of 100 μM solution of TNP, we have observed 87 and 89% decrease in the emission intensity for ZnPc**1** and ZnPc**2**, respectively. With further increase in the concentration, we have observed a plateau with no change in the emission intensity. Figure 4c shows the variation in quenching efficiency of various NACs toward ZnPcs. This study reveals that ZnPc**2** has superior quenching

DOI: 10.1021/acsomega.8b02394
ACS Omega 2019, 4, 6218−6228

performance (by 1.15 times) toward NACs, and both compounds show good selectivity toward TNP. As seen from Figure 5c, the emission intensity of ZnPc**2** was quenched by 60% as the concentration of TNT reached to 100 μM, whereas the quenching efficiencies of 2,4-DNT, 2,4-DNP, 4-NP, 4-NT, and NB are 22, 19, 9, 8, and 5%, respectively. It is also revealed that increase in the number of nitro groups enhances the electron deficiency in nitroaromatic molecules and thus the extent of fluorescence quenching. Additionally, the acidity of the phenolic group increases with an increase in the number of the nitro group, furnishing the formation of electrostatic interactions between ZnPcs and TNP. The trend in the quenching effect of ZnPcs follows the order: NM < NB < NT < NP < DNT < DNP < TNT < TNP. Figures S15 and S16 (Supporting Information) show changes in the emission spectra of ZnPcs treated with different nitro analytes. Figure S17 (Supporting Information) shows changes in the quenching efficiencies of ZnPcs at different concentrations of the nitro analytes. The LOD was obtained by measuring the emission intensities plotted against the concentration of TNP. The final LOD was measured using the formula LOD = 3.3 × σ/m, where σ is the standard deviation and m is the slope. From the experiments, it was found that the LODs of TNP were found to be 0.7 ± 0.1 and 1.1 ± 0.1 ppm (Figure S18, Supporting Information). The LODs are found to be lower than the standard detection limits of TNP described by Environmental Protection Agency in water.[36]

Further, the quenching behavior of ZnPcs with different nitro derivatives was quantitatively analyzed with the Stern−Volmer (SV) equation $I_o/I = 1 + K_{sv}[Q]$, where I_o and I represent the fluorescence emission intensity before and after addition of a quencher, [Q] is the molar concentration of the quencher, and K_{sv} is the SV rate constant. Figure 5 shows the SV plot of ZnPcs with different nitro derivatives. The I_o/I value is found to be linearly increased with increase in the concentration of TNP, indicating that the static quenching mechanism is more predominant. The quenching of emission is consistent with the photoinduced electron-transfer (PET) mechanism for which the electron present in the excited state of ZnPcs is transferred to the LUMO of the nitro analyte. Because the analyte is nonemissive, the emission is lost via nonradiative relaxation. Figure S19 (Supporting Information) shows the absorption and emission spectra of ZnPc**2** and TNP. From the spectra, it is observed that there is no overlap of emission of ZNPc**2**, and absorption of TNP indicates that the electron-transfer process is more predominant. Interestingly, for TNP, the SV plot shows a linear relationship at lower concentrations and exhibits an upward hill at higher concentrations, indicating that both static quenching and dynamic quenching exist for TNP. Remarkably, the upward curvature of I_o/I values was well fitted in the Perrin static quenching model $\ln(I_o/I) = K_{ap}[Q]$, where K_{ap} is the apparent static quenching constant. This type of static quenching occurs between randomly distributed fluorophores and quenchers that are in proximity. Fluorophore molecules in contact with Q at the instant of excitation will not fluoresce.[37]

The SV rate constants of ZnPcs treated with different nitro analytes are summarized in Table S2 (Supporting Information). ZnPc2 exhibits a high quenching rate constant of 2.02 × 10^5 for TNP and 1.40 × 10^5 for TNT. Other nitro derivatives were found to have relatively lower rate constants. ZnPc**1** shows 1.6 × 10^5 for TNP and 5.9 × 10^4 for TNT. To get more insights into the formation of adducts between the nitro derivatives and ZnPcs, we have carried out absorption titration experiments. The absorption spectra of ZnPc**2** upon addition of different concentrations of TNP show that the Q-band intensity increases along with the Soret band by formation of an intercalating adduct between ZnPc**2** and TNP (Figure S20, Supporting Information). As described earlier, ZnPc**2** tends to form aggregates; however, these aggregates were disrupted by TNP molecules by intercalation and exhibit ZnPc**2** in a monomeric form and lead to the formation of adducts. Because of the presence of regioisomers for ZnPc**1** and existence of monomeric forms, we have observed only decrease in the Q-band intensity. On the other hand, the Soret band intensity increased because of overlap in the absorption of Q-band and TNP at 375 nm.

To understand the effect of pH on the sensing behavior, we have carried out fluorescence titration experiments of ZnPc**2** with TNP by adjusting the pH of the solutions using 0.1 M NaOH and 0.1 M HCl.[38,39] Under high acidic conditions (pH ≈ 1−3), we have observed the formation of precipitates because of aggregation. Hence, titration experiments were performed from mild acidic to basic medium (pH 5−pH 12). Figure S21 (Supporting Information) shows change in the quenching behavior upon addition of different concentrations of TNP at pH 5 and pH 12. Upon addition of 2 μM TNP to ZnPc**2**, we have obtained the quenching efficiency of 29.4 and 41.8% at pH 5 and pH 12. At higher concentrations of TNP (200 μM), the quenching efficiencies of 95 and 93% were achieved. The variation in the quenching efficiencies arises because of different solvent environments. ZnPc**2** showed good response at two different pH regions, and the quenching efficiency is slightly lower than that of the neutral medium. At pH 5 and lower pH, the emission maxima dramatically decreased because of protonation of dimethylamine units of DMAP rendering ICT process. The quenching efficiency was strongly enhanced between pH 5 and pH 12 because the pH of the medium reaches neutral and basic medium because of formation of efficient electrostatic interactions of adduct formation between ZnPcs and TNP. Upon addition of TNP to ZnPc**2** (5×10^{-5}M) at pH-5, electrostatic interactions associated with the acid medium. Appreciable quenching efficiencies were achieved in slightly acidic, neutral, and basic media indicative of effective function as chemosensors in the wide pH ranges.

To further validate the electrostatic interactions between ZnPcs and TNP, we have performed ^{1}H NMR studies upon addition of different concentrations of TNP to ZnPc**2** (Figure S22, Supporting Information). Upon addition of TNP, we have observed two significant characteristic features. In the first step, ZnPc**2** undergoes protonation at dimethylamino groups, which hinders the intramolecular charge transfer from dimethylamino groups to the macrocycle core and further leads to electrostatic interaction between the protonated form and the picrate anion. Second, because of the highly acidic character of the phenolic moiety in TNP, the pyridinium nitrogen may also get protonated at higher concentrations, furnishing high fluorescence quenching. The $-N(CH_3)_2$ proton signal at δ 3.22 ppm undergoes a downfield shift of $\Delta\delta$ = 0.06 ppm on addition of TNP, which demonstrates the protonation of the dimethylamine unit. The doublet peak of *meta* phenyl ring protons of the DMAP unit at δ 7.095 ppm converted into multiplets with a downfield shift of δ 0.03 ppm, whereas the doublet peak of the *ortho* phenyl ring protons at δ 8.289 ppm converted into triplets at 1:0.5 equivalent of TNP. At higher

DOI: 10.1021/acsomega.8b02394
ACS Omega 2019, 4, 6218−6228

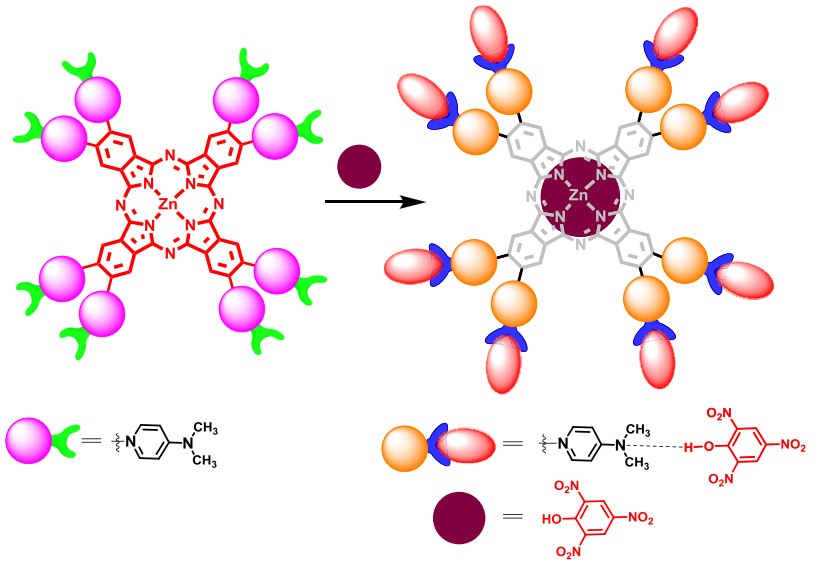

Figure 6. Schematic illustration of possible mode of interactions between ZnPc**2** and TNP.

concentrations of TNP, the triplet peaks further interconverted to multiplets with a downfield shift of δ 0.09 ppm. On the other hand, we have observed a newly generated broad singlet peak appearing at δ 10.781 ppm equivalent of TNP with a more downfield shift of δ 11.438 ppm, leading to the protonation of quaternary pyridinium nitrogen of ZnPc**2**. The broad proton signals of ZnPc**2**-α-H become sharper with a split in the downfield shift, indicating $\pi-\pi$ stacking interaction between them by formation of the ZnPc**2**-TNP adduct.

To further understand the role of electrostatic interactions, a control experiment was carried out by methylation on ZnPcs using dimethyl sulfate and treated with different nitro analytes.[32] Under similar experimental conditions, the methylated ZnPc**2** shows 59% decrease in the emission intensity upon addition of 100 μM of TNP, which is 30% less than ZnPc**2**, as the dimethylamino moiety is no longer available for ICT owing to its methylation. We have observed a similar behavior for other nitro compounds treated with ZnPc**1**.

Figure S23 (Supporting Information) shows the quenching efficiency of methylated ZnPcs treated with different nitro compounds. From these results, it is clearly evident that the picrate anion interacts with the protonated form of *N*,*N*′-dimethylamine and pyridinium moieties through electrostatic interaction along with $\pi-\pi$ interactions, playing a major driving force for the fluorescence quenching process.[40] Figure 6 shows the schematic representation of possible mode of interactions between ZnPc**2** and PA.

Toward the real-time applications, selective detection of the analytes is quite important. Hence, the selectivity of ZnPcs toward the detection of TNP in water in presence of other nitroanalytes was investigated by the competitive fluorescence quenching assay. In a typical experiment, the emission spectrum of ZnPcs was initially recorded. To this solution, TNT (10 μM) solution was added and allowed to effectively access interactions with ZnPcs, and the emission spectra were recorded. We have observed no significant changes in the fluorescence quenching upon addition of TNT. To this solution, the same quantity of TNP was added, which resulted in a significant change in the fluorescence quenching efficiency. The experiment was repeated upon addition of different concentration cycles of TNT and TNP.

We have observed that with an increase in the concentration of TNP, fluorescence quenching significantly decreased. The experiment was repeated for other nitro analytes with the addition of TNP solutions, and change in the quenching efficiency is summarized in Figure 7. The stepwise decrease in

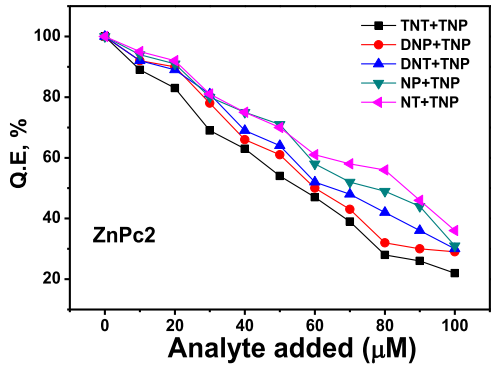

Figure 7. Competitive fluorescence quenching efficiency of ZnPc**2** upon addition of different nitro analytes, followed by TNP.

the quenching efficiency clearly demonstrates the unprecedented selectivity of ZnPc**2** toward TNP in the presence of other competitive nitro analytes in aqueous medium. Similar trend in the quenching efficiency of ZnPc**1** was observed in the presence of other competitive nitro analytes, furnishing its high selectivity toward TNP over all the congener nitro analytes.

For field applicability and real-time analysis, the sensing behavior was studied in drinking water and river water samples. Upon addition of drinking water (obtained from SRMIST common source point) to ZnPc**2**, we have not observed any significant changes in emission spectra, indicating that drinking water does not have trace amounts of TNP. We have also tested river water obtained from the banks of Palar river near Chengalpattu, Tamil Nadu. The river water was used as an analyte and a solvent medium. In the first experiment, different amounts of river water are directly added to the ZnPc**2** solution, and changes in the emission maxima are monitored.

DOI: 10.1021/acsomega.8b02394
ACS Omega 2019, 4, 6218−6228

Upon addition of 100 μL of river water, we have observed 11% quenching of emission maxima (Figure S24a, Supporting Information). In the second experiment, we have prepared the stock solution of TNP using river water and treated with ZnPc**2**. Interestingly, upon addition of 150 μM of TNP, we have observed 84% quenching efficiency that reflects the potential applicability of ZnPc**2** for the real-time analysis (Figure S24b, Supporting Information).

Toward the solid-state sensors for explosives, we have prepared thin films of ZnPcs by the spin-coating method on quartz substrates as described earlier.[41] The solid-state emission spectra of ZnPcs in thin films showed that the peaks are slightly broadened and red-shifted by 8 ± 2 nm compared to that in aqueous media. The fluorescence response of thin films upon exposure to saturated vapors of different nitro compounds was monitored as a function of time. Interestingly, we have observed that ZnPcs exhibit high fluorescence quenching toward TNP vapors. Figure 8a shows

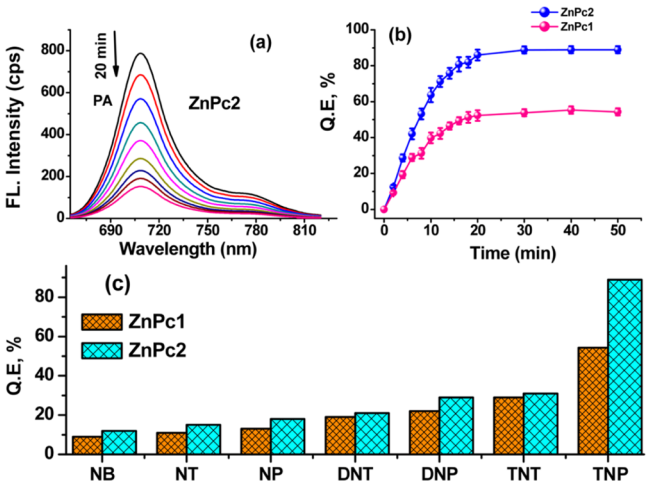

Figure 8. (a) Change in the fluorescence intensity of ZnPc**2** upon exposure to the saturated vapors of TNP at different time intervals. (b) Change in the quenching efficiency of ZnPcs with TNP vapors at different time intervals. (c) Quenching efficiency of ZnPcs to different vapors of NACs.

change in the emission intensity of ZnPc**2** to TNP vapors. The fluorescence intensity gradually decreased with respect to the time of exposure without change in the position of peak maxima. The emission intensity remarkably decreased initially and showed slower response for the prolonged time of exposure. Upon exposure of thin films to TNP vapors for 240 s, ZnPc**2** exhibits the quenching efficiencies of 28.6, 9.8, 9.2, and 7.5% toward TNP, TNT, DNP, and DNT vapors, respectively. Upon exposure of thin films to TNP vapors for 18 mins, we have observed the quenching efficiency of 80.7% and reached a plateau. With further increase in the exposure time, no remarkable changes in emission were observed (Figure 8b). ZnPc**1** exhibits ~49.1% decrease in the quenching efficiency.

The overall order of quenching efficiency was found to be TNP > TNT ≈ DNP > DNT > NP > NT > NB, indicating that ZnPc**2** exhibits high selectivity toward TNP and is found to have 1.6 times higher sensitivity than ZnPc**1** (Figure 8c). The variation in the sensitivity may arise due to variations in the structures of ZnPc and morphology of the films in the solid state. The DFT-optimized structure of ZnPc**2** shows a bowl shape structure, which allows for easy encapsulation of guest molecules, whereas ZnPc**1** exhibits a nonplanar distorted structure. The scanning electron microscopy image of the films shows spherical and ordered crystalline structures for ZnPc**1** and ZnPc**2**, respectively (Figure S25, Supporting Information). The variations in the morphology of ZnPcs and increase in the number of DMAP units facilitate to have better interactions and furnish variations in the selectivity toward NACs vapors. The ordered crystalline morphology provides large contact area to capture more analyte molecules and trigger larger signal change. Although the vapor pressure of NB (4×10^5 ppb) and TNT (7.7×10^{-3} ppb) is higher than that of TNP (7.7×10^{-3} ppb), ZnPcs exhibit good interactions through $\pi-\pi$ and electrostatic interactions with the acidic nature of the TNP vapors.

Figure 9 shows confocal fluorescence microscopy image of ZnPcs before and after exposure to the vapors of TNP. The red

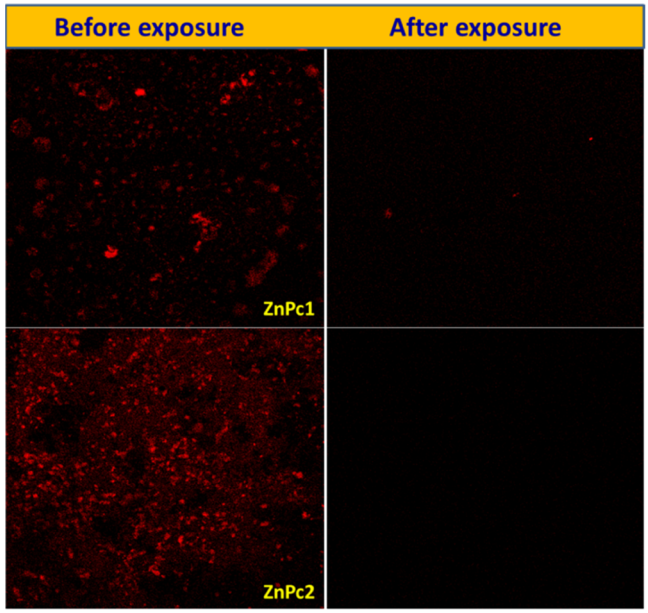

Figure 9. Confocal fluorescence microscopy images of ZnPc films exposed to saturated vapors of TNP (scale bar 20 μm).

fluorescence in the films is completely diminished in ZnPc**2** films, indicating its potential use to design infrared-based fluorescence detectors because of their diffusion ability. The reversibility and recycling ability of the films were further evaluated by exposing the films to TNP vapors for 15 min and washed with methanol and dried under N_2 gas flow for 10 min. From Figure S26 (Supporting Information), the emission intensity of the virgin film decreased upon exposure to TNP vapors and retains the emission after washing with methanol. We have observed only 6% decrease in the emission intensity even after 8 cycles and presumably attain the efficient quenching process, indicating that ZnPc films exhibit high reversibility and recycling ability.[42]

Our major research emphasis is to design the novel molecular materials toward the detection of explosive compounds and to in situ convert them into fine chemicals. Nitrophenolic compounds are known to undergo reduction in the presence of $NaBH_4$ and other reducing agents to form a corresponding aminophenol thermodynamically.[43] Some of MPcs and double decker lanthanide Pcs were used directly and

DOI: 10.1021/acsomega.8b02394
ACS Omega 2019, 4, 6218−6228

impregnated with TiO_2 and other metal oxides toward the photocatalytic degradation in aqueous suspension.[44−46] In this regard, we anticipated that developed ZnPcs have the ability toward selective detection of TNP and could also possibly act as a photocatalyst for the degradation of TNP. In a typical experiment, TNP was mixed with $NaBH_4$ in a 3 mL quartz cuvette in ethanol solution. The solutions immediately turned bright yellow (λ_{abs} = 396 nm) from light yellow (λ_{abs} = 354 nm), which indicates the formation of phenolate ions. ZnPc**2** (3 mg) was added to the resulting solution and irradiated under white light (9.0 mW cm^{-2}). Changes in the absorbance were monitored by an absorption spectrophotometer.

The absorption maxima at ∼396 nm is gradually decreased as a function of time with appearance of a new absorption peak at 263 nm, indicating the formation of 2,4,6-triaminophenol (TAP).[47] Figure 10 shows that the absorption at ∼396 nm

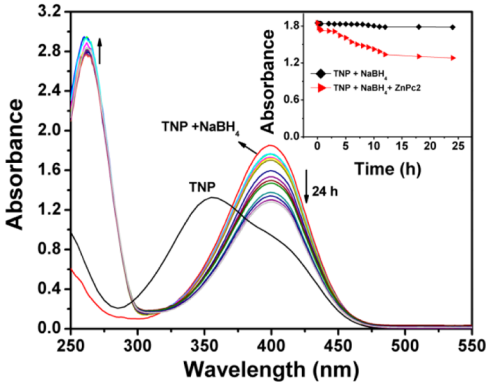

Figure 10. Change in the absorption spectra of TNP, followed by addition of $NaBH_4$ and ZnPc**2** in ethanol solution under the irradiation of white light.

decreases and shows the conversion rate of 30% for an exposure period of 24 h. With further increase in the exposure time, we have not observed any substantial changes in the conversion process. A control experiment was carried out without addition of ZnPc**2** to understand the role of a photocatalyst. In the absence of ZnPc**2**, we have not observed any significant changes in the absorption maxima at ∼396 nm, indicating the significant role of ZnPc**2** as a photocatalyst in the reduction process by formation of singlet oxygen ($^1O_2$). Further, optimization of the reaction conditions with an increase in the dose of the catalyst, power, and hydrogen source for phenolate to improve the catalytic conversion of nitro phenol analytes with faster reaction kinetics in the reduction process without altering the sensing ability and selectivity of ZnPcs is under investigation.

CONCLUSIONS

Novel water-soluble ZnPcs with four and eight DMAP units at the periphery were synthesized and characterized. The photophysical properties, singlet oxygen generation, and stability/photostability were investigated. Increase in the number of DMAP groups on ZnPc enhances the conjugation and showed a significant effect in the photophysical properties. ZnPc**2** exhibits J-type aggregates at higher concentrations, and both compounds show high singlet oxygen generation. Fluorescence studies of ZnPc**1** and ZnPc**2** treated with different NACs show a fluorescence quenching behavior with unprecedented selectivity toward TNP in the aqueous medium. The quenching rate constants were found to be 1.6 × 10^5 and 2.02 × 10^5 for ZnPc**1** and ZnPc**2** with LODs of 1.1 ± 0.1 and 0.7 ± 0.1 ppm, respectively. By corroborating fluorescence and NMR studies, the PET process through donor−acceptor $\pi-\pi$ interactions and electrostatic interaction between the dimethylamine unit of DMAP and TNP is predominant for the quenching process. The vapor-phase studies demonstrate that ZnPc**2** shows 1.6 times higher sensitivity than ZnPc**1**, which may be due to variation in the morphology in the solid state, and the bowl shape of ZnPc**2** furnishes cavity-based selectivity in terms of the size and efficient interaction of nitro analyte vapors. The preliminary heterogeneous photocatalytic studies demonstrate that developed compounds show 31% of catalytic activity in the reduction of TNP to corresponding TAP. This work provides an interesting perspective on the elaboration of unique fluorescent molecular systems, which can show selective sensing of specific nitro analytes and convert them into useful chemicals. Current efforts are now being made toward the design of fluorescent receptors, which act as selective sensors as well as heterogeneous catalyst/photocatalysts in the efficient reduction of nitro analytes.

MATERIALS AND METHODS

All chemicals of analytical grade were obtained from Sigma-Aldrich and used as received. Solvents were purified by distillation, and reagents were used without further purification. The ^1H and ^{13}C NMR spectra were recorded in a Bruker NMR equipment (300.13 and 75.47 MHz). Chemical shifts are reported in parts per million. The final mass of the compounds was confirmed by a MALDI-Micromass Q-TOF2 equipment. UV−vis spectra were recorded on a Cary 5000 UV−vis−NIR spectrophotometer. Steady-state fluorescence emission studies were carried out on a Jobin-Yvon FluoroMax 3 spectrofluorometer. Fluorescence quantum yields were determined using the unsubstituted ZnPc (Φ_F = 0.20) as the reference.[31] Time-resolved fluorescence measurements were carried out with the TCSPC method with a picosecond LED (635 nm, pulse width <200 ps) being used to excite the samples. Photostability, stability, photobleaching, and singlet oxygen studies were carried out as described in the literature.[32] Thin films of ZnPcs were prepared by a spin-coating method by dissolving 1 mg of compound in 200 μL, which was spin-coated on the quartz substrate. Thin films were annealed at 70 °C overnight and stored in the vacuum desiccator. Solid-state fluorescence quenching studies were performed by exposing the films to the saturated vapors of nitro analytes, and emission data were collected by the front face method. Confocal microscopic images of thin films were obtained in LSM 710 Carl Zeiss laser scanning microscope. **Caution**: TNP, TNT, and other NACs used in the present study have explosive nature and should be handled only in small quantities.

ASSOCIATED CONTENT

Supporting Information

The Supporting Information is available free of charge on the ACS Publications website at DOI: 10.1021/acsomega.8b02394.

^1H, ^{13}C NMR, and mass spectrum of phthalonitriles and ZnPcs; aggregation, stability, and photostability; fluorescence lifetime and fluorescence quenching behavior

DOI: 10.1021/acsomega.8b02394
ACS Omega 2019, 4, 6218−6228

with NACs in solution and vapor phases, and NMR titration and detection limit calculations (PDF)

AUTHOR INFORMATION

Corresponding Author

*E-mail: nvenkat83@gmail.com.

ORCID

N. Venkatramaiah: 0000-0003-0235-2707

Author Contributions

The manuscript was written through contributions of all authors. All authors have given approval to the final version of the manuscript.

Notes

The authors declare no competing financial interest.

ACKNOWLEDGMENTS

S.K. acknowledges SRMIST and CSIR for junior research fellowship (JRF). N.V. acknowledges financial assistance from the Department of Science & Technology, Ministry of Science & Technology (DST-FIST) for infrastructure development [SR//FST/CSI-266/2015(C)] to SRMIST. The authors also acknowledge the photoluminescence spectrometer facility of SRMIST. We thank Prof. J. P. C. Tome and Prof. Filipe Paz, Department of Chemistry, University of Aveiro, Portugal, for useful discussions.

REFERENCES

(1) Akhavan, J. *The Chemistry of Explosives*; Royal Society of Chemistry: Cambridge, 2004.

(2) Pohanish, R. P. *Handbook of Toxic and Hazardous Chemicals and Carcinogens*, 6th ed.; William Andrew: New York, 2012.

(3) Wyman, J. F.; Serve, M. P.; Hobson, D. W.; Lee, L. H.; Uddin, D. E. Acute toxicity, distribution, and metabolism of 2,4,6-trinitrophenol (picric acid) in Fischer 344 rats. *J. Toxicol. Environ. Health* **1992**, *37*, 313.

(4) Hill, H. H.; Simpson, G. Capabilities and limitations of ion mobility spectrometry for field screening applications. *Field Anal. Chem. Technol.* **1997**, *1*, 119−134.

(5) Moore, D. S. Instrumentation for trace detection of high explosives. *Rev. Sci. Instrum.* **2004**, *75*, 2499−2512.

(6) Walsh, M. Determination of nitroaromatic, nitramine, and nitrate ester explosives in soil by gas chromatography and an electron capture detector. *Talanta* **2001**, *54*, 427−438.

(7) Zhang, H.-X.; Hu, J.-S.; Yan, C.-J.; Jiang, L.; Wan, L.-J. Functionalized carbon nanotubes as sensitive materials for electrochemical detection of ultra-trace 2,4,6-trinitrotoluene. *Phys. Chem. Chem. Phys.* **2006**, *8*, 3567−3572.

(8) Goldman, E. R.; Anderson, G. P.; Lebedev, N.; Lingerfelt, B. M.; Winter, P. T.; Patterson, C. H.; Mauro, J. M. Analysis of aqueous 2,4,6-trinitrotoluene (TNT) using a fluorescent displacement immunoassay. *Anal. Bioanal. Chem.* **2003**, *375*, 471−475.

(9) Guan, W.; Zhou, W.; Lu, J.; Lu, C. Luminescent films for chemo- and biosensing. *Chem. Soc. Rev.* **2015**, *44*, 6981−7009.

(10) Lin, H.; Suslick, K. S. A Colorimetric Sensor Array for Detection of Triacetone Triperoxide Vapor. *J. Am. Chem. Soc.* **2010**, *132*, 15519−15521.

(11) Yang, J.-S.; Swager, T. M. Porous Shape Persistent Fluorescent Polymer Films: An Approach to TNT Sensory Materials. *J. Am. Chem. Soc.* **1998**, *120*, 5321−5322.

(12) Lan, A.; Li, K.; Wu, H.; Olson, D. H.; Emge, T. J.; Ki, W.; Hong, M.; Li, J. A Luminescent Microporous Metal-Organic Framework for the Fast and Reversible Detection of High Explosives. *Angew. Chem., Int. Ed.* **2009**, *48*, 2334−2338.

(13) Yao, J.; Yang, M.; Duan, Y. Chemistry, Biology, and Medicine of Fluorescent Nanomaterials and Related Systems: New Insights into Biosensing, Bioimaging, Genomics, Diagnostics, and Therapy. *Chem. Rev.* **2014**, *114*, 6130.

(14) Shanmugaraju, S.; Mukherjee, P. S. π-Electron rich small molecule sensors for the recognition of nitroaromatics. *Chem. Commun.* **2015**, *51*, 16014−16032.

(15) Venkatramaiah, N.; Kumar, S.; Patil, S. Fluoranthene based fluorescent chemosensors for detection of explosive nitroaromatics. *Chem. Commun.* **2012**, *48*, 5007−5009.

(16) Wang, Y.; La, A.; Brückner, C.; Lei, Y. FRET- and PET-based sensing in a single material: expanding the dynamic range of an ultrasensitive nitroaromatic explosives assay. *Chem. Commun.* **2012**, *48*, 9903−9905.

(17) Maiti, K.; Mahapatra, A. K.; Gangopadhyay, A.; Maji, R.; Mondal, S.; Ali, S. S.; Das, S.; Sarkar, R.; Datta, P.; Mandal, D. Simple Bisthiocarbonohydrazone as a Sensitive, Selective, Colorimetric, and Ratiometric Fluorescent Chemosensor for Picric Acids. *ACS Omega* **2017**, *2*, 1583−1593.

(18) Huang, W.; Bender, M.; Seehafer, K.; Wacker, I.; Schröder, R. R.; Bunz, U. H. F. A Tetraphenylethene-Based Polymer Array Discriminates Nitroarenes. *Macromolecules* **2018**, *51*, 1345−1350.

(19) Xu, Y.; Li, B.; Li, W.; Zhao, J.; Sun, S.; Pang, Y. "ICT-not-quenching" near infrared ratiometric fluorescent detection of picric acid in aqueous media. *Chem. Commun.* **2013**, *49*, 4764−4766.

(20) Nagarkar, S. S.; Desai, A. V.; Samanta, P.; Ghosh, S. K. Aqueous phase selective detection of 2,4,6-trinitrophenol using a fluorescent metal-organic framework with a pendant recognition site. *Dalton Trans.* **2015**, *44*, 15175−15180.

(21) Bhalla, V.; Kaur, S.; Vij, V.; Kumar, M. Mercury-Modulated Supramolecular Assembly of a Hexaphenylbenzene Derivative for Selective Detection of Picric Acid. *Inorg. Chem.* **2013**, *52*, 4860−4865.

(22) Ng, D. K. P.; Jiang, J. Sandwich-type heteroleptic phthalocyaninato and porphyrinato metal complexes. *Chem. Soc. Rev.* **1997**, *26*, 433−442.

(23) Yslas, E. I.; Rivarola, V.; Durantini, E. N. Synthesis and photodynamic activity of zinc(II) phthalocyanine derivatives bearing methoxy and trifluoromethylbenzyloxy substituents in homogeneous and biological media. *Bioorg. Med. Chem.* **2005**, *13*, 39−46.

(24) Jiang, X.-J.; Lo, P.-C.; Yeung, S.-L.; Fong, W.-P.; Ng, D. K. P. A pH-responsive fluorescence probe and photosensitiser based on a tetraamino silicon(IV) phthalocyanine. *Chem. Commun.* **2010**, *46*, 3188.

(25) Çakır, D.; Göksel, M.; Çakır, V.; Durmuş, M.; Biyiklioglu, Z.; Kantekin, H. Amphiphilic zinc phthalocyanine photosensitizers: synthesis, photophysicochemical properties and in vitro studies for photodynamic therapy. *Dalton Trans.* **2015**, *44*, 9646.

(26) Ikeuchi, T.; Mack, J.; Nyokong, T.; Kobayashi, N.; Kimura, M. Aggregation Control of Robust Water-Soluble Zinc(II) phthalocyanine-Based Photosensitizers. *Langmuir* **2016**, *32*, 11980−11985.

(27) Venkatramaiah, N.; Pereira, P. M. R.; Almeida Paz, F. A.; Ribeiro, C. A. F.; Fernandes, R.; Tomé, J. P. C. Dual functionality of phosphonic-acid-appended phthalocyanines: inhibitors of urokinase plasminogen activator and anticancer photodynamic agents. *Chem. Commun.* **2015**, *51*, 15550.

(28) Öztürk, Z. Z.; Kılınç, N.; Atilla, D.; Gürek, A. G.; Ahsen, V. Recent studies chemical sensors based on phthalocyanines. *J. Porphyrins Phthalocyanines* **2009**, *13*, 1179−1187.

(29) Venkatramaiah, N.; Rocha, D. M. G. C.; Srikanth, P.; Almeida Paz, F. A.; Tomé, J. P. C. Synthesis and photophysical characterization of dimethylamine-derived Zn(II)phthalocyanines: exploring their potential as selective chemosensors for trinitrophenol. *J. Mater. Chem. C* **2015**, *3*, 1056.

(30) Thorne, P. G.; Jenkins, T. F. A field method for quantifying ammonium picrate and picric acid in soil. *Field Anal. Chem. Technol.* **1997**, *1*, 165.

(31) Ogunsipe, A.; Chen, J.-Y.; Nyokong, T. Photophysical and photochemical studies of zinc(II) phthalocyanine derivatives-effects of substituents and solvents. *New J. Chem.* **2004**, *28*, 822−827.

(32) Lourenço, L. M. O.; Rocha, D. M. G. C.; Ramos, C. I. V.; Gomes, M. C.; Almeida, A.; Faustino, M. A. F.; Almeida Paz, F. A.;

DOI: 10.1021/acsomega.8b02394
ACS Omega 2019, 4, 6218−6228

Neves, M. G. P. M. S.; Cunha, Â.; Tomé, J. P. C. Photoinactivation of Planktonic and Biofilm Forms of Escherichia coli Through the Action of Cationic Zinc(II) Phthalocyanines. *ChemPhotoChem* **2019**, DOI: 10.1002/cptc.201900020.
(33) Görlach, B.; Dachtler, M.; Glaser, T.; Albert, K.; Hanack, M. Synthesis and Separation of Structural Isomers of 2(3),9(10),16(17),23(24)-Tetrasubstituted Phthalocyanines. *Chem.—Eur. J.* **2001**, *7*, 2459−2465.
(34) Tanielian, C.; Wolff, C.; Esch, M. Singlet Oxygen Production in Water: Aggregation and Charge-Transfer Effects. *J. Phys. Chem.* **1996**, *100*, 6555−6560.
(35) Frisch, M. J.; Trucks, G. W.; Schlegel, H. B.; Scuseria, G. E.; Robb, M. A.; Cheeseman, J. R.; Scalmani, G.; Barone, V.; Petersson, G. A.; Nakatsuji, H.; Li, X.; Caricato, M.; Marenich, A. V.; Bloino, J.; Janesko, B. G.; Gomperts, R.; Mennucci, B.; Hratchian, H. P.; Ortiz, J. V.; Izmaylov, A. F.; Sonnenberg, J. L.; Williams-Young, D.; Ding, F.; Lipparini, F.; Egidi, F.; Goings, J.; Peng, B.; Petrone, A.; Henderson, T.; Ranasinghe, D.; Zakrzewski, V. G.; Gao, J.; Rega, N.; Zheng, G.; Liang, W.; Hada, M.; Ehara, M.; Toyota, K.; Fukuda, R.; Hasegawa, J.; Ishida, M.; Nakajima, T.; Honda, Y.; Kitao, O.; Nakai, H.; Vreven, T.; Throssell, K.; Montgomery, J. A., Jr.; Peralta, J. E.; Ogliaro, F.; Bearpark, M. J.; Heyd, J. J.; Brothers, E. N.; Kudin, K. N.; Staroverov, V. N.; Keith, T. A.; Kobayashi, R.; Normand, J.; Raghavachari, K.; Rendell, A. P.; Burant, J. C.; Iyengar, S. S.; Tomasi, J.; Cossi, M.; Millam, J. M.; Klene, M.; Adamo, C.; Cammi, R.; Ochterski, J. W.; Martin, R. L.; Morokuma, K.; Farkas, O.; Foresman, J. B.; Fox, D. J. *Gaussian 16, Revision B.01*; Gaussian, Inc.: Wallingford CT, 2016.
(36) Thomas, S. W.; Joly, G. D.; Swager, T. M. Chemical Sensors Based on Amplifying Fluorescent Conjugated Polymers. *Chem. Rev.* **2007**, *107*, 1339.
(37) Valeur, B. *Molecular Fluorescence: Principles and Applications*; Wiley-VCH Verlag GmbH: Weinheim, 2001.
(38) Fan, Y. Z.; Zhang, Y.; Li, N.; Liu, S. G.; Liu, T.; Li, N. B.; Luo, H. Q. A facile synthesis of water-soluble carbon dots as a label-free fluorescent probe for rapid, selective and sensitive detection of picric acid. *Sens. Actuators, B* **2017**, *240*, 949−955.
(39) Jigyasa; Kaur Rajput, J. "ON-OFF" novel fluorescent chemosensors based on nanoaggregates of triaryl imidazoles for superselective detection of nitro-explosive trinitrophenol in multiple solvent systems. *Sens. Actuators, B* **2018**, *259*, 990−1005.
(40) Zhang, K.; Yang, L.; Zhu, H.; Ma, F.; Zhang, Z.; Wang, S. Selective visual detection of trace trinitrotoluene residues based on dual-color fluorescence of graphene oxide-nanocrystals hybrid probe. *Analyst* **2014**, *139*, 2379−2385.
(41) Kumar, S.; Venkatramaiah, N.; Patil, S. Fluoranthene Based Derivatives for Detection of Trace Explosive Nitroaromatics. *J. Phys. Chem. C* **2013**, *117*, 7236−7245.
(42) Ko, J. H.; Moon, J. H.; Kang, N.; Park, J. H.; Shin, H.-W.; Park, N.; Kang, S.; Lee, S. M.; Kim, H. J.; Ahn, T. K.; Lee, J. Y.; Son, S. U. Engineering of Sn-porphyrin networks on the silica surface: sensing of nitrophenols in water. *Chem. Commun.* **2015**, *51*, 8781−8784.
(43) Pozun, Z. D.; Rodenbusch, S. E.; Keller, E.; Tran, K.; Tang, W.; Stevenson, K. J.; Henkelman, G. A Systematic Investigation of p-Nitrophenol Reduction by Bimetallic Dendrimer Encapsulated Nanoparticles. *J. Phys. Chem. C* **2013**, *117*, 7598−7604.
(44) Verma, P. K.; Bala, M.; Thakur, K.; Sharma, U.; Kumar, N.; Singh, B. Iron and Palladium(II) phthalocyanines as Recyclable Catalysts for Reduction of Nitroarenes. *Catal. Lett.* **2014**, *144*, 1258−1267.
(45) Chao, C.-G.; Bergbreiter, D. E. Highly organic phase soluble polyisobutylene-bound cobalt phthalocyanines as recyclable catalysts for nitroarene reduction. *Catal. Commun.* **2016**, *77*, 89−93.
(46) Mele, G.; Garcìa-Lòpez, E.; Palmisano, L.; Dyrda, G.; Słota, R. Photocatalytic Degradation of 4-Nitrophenol in Aqueous Suspension by Using Polycrystalline TiO_2 Impregnated with Lanthanide Double-Decker phthalocyanine Complexes. *J. Phys. Chem. C* **2007**, *111*, 6581−6588.
(47) Devi, T. B.; Ahmaruzzaman, M. Bio-inspired facile and green fabrication of Au@Ag@AgCl core-double shells nanoparticles and their potential applications for elimination of toxic emerging pollutants: A green and efficient approach for wastewater treatment. *Chem. Eng. J.* **2017**, *317*, 726−741.

DOI: 10.1021/acsomega.8b02394
ACS Omega 2019, 4, 6218−6228